Short communication

Enhanced room temperature stretch formability of AZ31B magnesium alloy sheet by laser shock peening

Bo Mao[a], Bin Li[b], Dong Lin[c], Yiliang Liao[a],*

[a] Department of Mechanical Engineering, University of Nevada, Reno, Reno, NV, 89557, USA
[b] Department of Chemical and Materials Engineering, University of Nevada, Reno, Reno, NV, 89557, USA
[c] Department of Industrial and Manufacturing Systems Engineering, Kansas State University, Manhattan, KS, 66506, USA

A B S T R A C T

Laser shock peening (LSP) experiments were conducted on an AZ31B Mg alloy sheet. The results show that the room-temperature stretch formability of Mg alloy sheet can be enhanced by LSP, particularly through an integrated texture weakening and grain refinement effect induced by the laser shock loading.

1. Introduction

As the lightest structural metals, magnesium (Mg) and its alloys possess high specific strength, good recyclability, and desirable biocompatibility [1] which make them attractive for broad industrial applications [2]. However, applications of Mg alloys are restricted by their poor formability at room temperature [3]. This challenge is associated with their hexagonal closed packed (HCP) structure which present insufficient independent slip systems [4]. Wrought Mg alloys also present strong basal texture, giving rise to anisotropic deformation behavior [5].

Several strategies have been developed to enhance the room-temperature formability of Mg alloys, either through alloying or processing. The addition of rare earth (RE) alloying elements, such as Ce [6], Gd [7], Y [8], and Ca [9], has been proved to be efficient in improving the formability [10,11]. However, the addition of rare earth elements renders the Mg alloys expensive and incompatible with recycling constraints [12]. On the other hand, processing-oriented options, such as pre-compression [13], high temperature rolling [14], differential speed rolling [15], electo-plastic differential speed rolling [16], cross-wavy bending [17], and equal channel angular processing [18], provide effective alternatives with advantages of bulk processing, high controllability, and large scale manufacturing. From a metallurgical perspective, the formability of Mg alloys can be improved either by basal texture weakening or grain refinement. A weakened basal texture allows more homogeneous plastic deformation and refined grains promotes grain boundary sliding (GBS) which provides additional deformation mode [19,20].

In recent years, laser shock peening (LSP) emerges as a promising technology to improve the engineering performance of Mg alloys by enhancing their surface strength [21], biocompatibility [22], fatigue life [23], tribological performance [24] and corrosion resistance [25]. Compared with processing methods mentioned above, LSP is exceptional due to its capability of processing samples with complex geometries and generating deep plastic deformation without degrading the surface quality [26,27]. Our recent studies indicate that LSP of Mg alloys leads to the generation of a high density of {10$\bar{1}$2} extension twins, leading to a crystallographic lattice orientation of 86.3° around 1$\bar{2}$10 zone axis [28,29]. The lattice reorientation induced by pre-twinning provides an approach to tailor the basal texture of Mg alloys [30,31]. In addition, grain refinement by LSP of metallic materials has been extensively reported [23,32,33]. All these findings indicate that LSP could potentially enhance the formability of Mg alloys.

In this study the applicability of LSP to improve the room-temperature stretch formability of Mg alloy sheet is investigated. LSP experiments were conducted on an AZ31B Mg alloy. The microstructure was characterized using optical microscopy (OM) and electron backscattered diffraction (EBSD) microscopy. Erichsen tests were carried out to evaluate the stretch formability. The results show that LSP can provide a combined texture weakening and grain refinement, leading to improved room-temperature stretch formability of the Mg alloy sheet.

Table 1
Chemical composition of AZ31B Mg alloy (wt %).

Element	Al	Zn	Mn	Si	Cu	Ca	Fe	Ni	Mg
Weight	3.1	1.0	0.2	0.1	0.03	0.02	0.002	0.005	Balance

2. Experiments

A commercial rolled AZ31B Mg alloy block was used for experiments. The chemical composition of the block is listed in Table 1. The sheet samples were machined to a thickness of 1 mm. The surfaces of the sheet samples were perpendicular to normal direction (ND). Before LSP, the samples were grinded using SiC sandpapers, followed by fine polishing using 3 μm diamond suspension. Afterwards, all samples were annealed at 300 °C for 4 h in a vacuum furnace to remove the possible artifacts induced by machining or polishing.

A schematic of the setup of the LSP process is shown in Fig. 1a. A Q-switched Nd-YAG laser (1064 nm wavelength and 7 ns pulse width), was used to deliver the laser energy. The laser beam diameter was 2 mm. Black tape with a thickness of 100 μm and BK7 glass were used as the ablative coating and transparent confinement, respectively. The LSP scan path is schematically illustrated in Fig. 1b. The distance between two neighboring spots is 1 mm and the overlapping ratio is 39%. LSP was performed along ND to process the whole surfaces of samples. During LSP, the nanosecond pulsed laser energy is absorbed by ablative

coating, leading to the generation of a high shockwave pressure ($\sim$GPa) propagating into the sample [26,34,35]. The temporal evolution of laser shockwave pressure as affected by the laser intensity can be estimated by Fabbro's model [36] (Fig. 1c). For instance, given a laser intensity of 4 GW/cm^2, the peak shock pressure reaches 3.5 GPa.

The room-temperature stretch formability of laser processed samples was evaluated by the Erichsen tests. A schematic configuration of Erichsen test is illustrated in Fig. 1d. The diameter of the lower mold and upper mold were 15 and 17 mm, respectively. An Instron testing machine was used to control the forming speed and record the load vs. displacement behavior. The forming load was applied on a hemispherical shape punch with a diameter of 10 mm at a constant speed of 0.01 mm/s. The movement of the punch stopped as cracks initiated (indicated by a 10% drop of the maximum load) on the lower surface (LSP processed surface) of the sample. The values of limit dome height (LDH), i.e., stretch formability, defined as the depth of the punch at fracture initiation, were then measured. To investigate the effect of LSP on the mechanical properties of Mg alloys, tensile tests were carried out using the "dog-bone" samples with a gauge area of 16 mm (RD) by 6 mm (TD) and a thickness of 2 mm (ND) machined from the Mg block, as shown in Fig. 1e. Both sides of the gauge area of the samples subjected to tensile tests were LSP processed. The strain rates were set as 0.0005/s in the tensile tests.
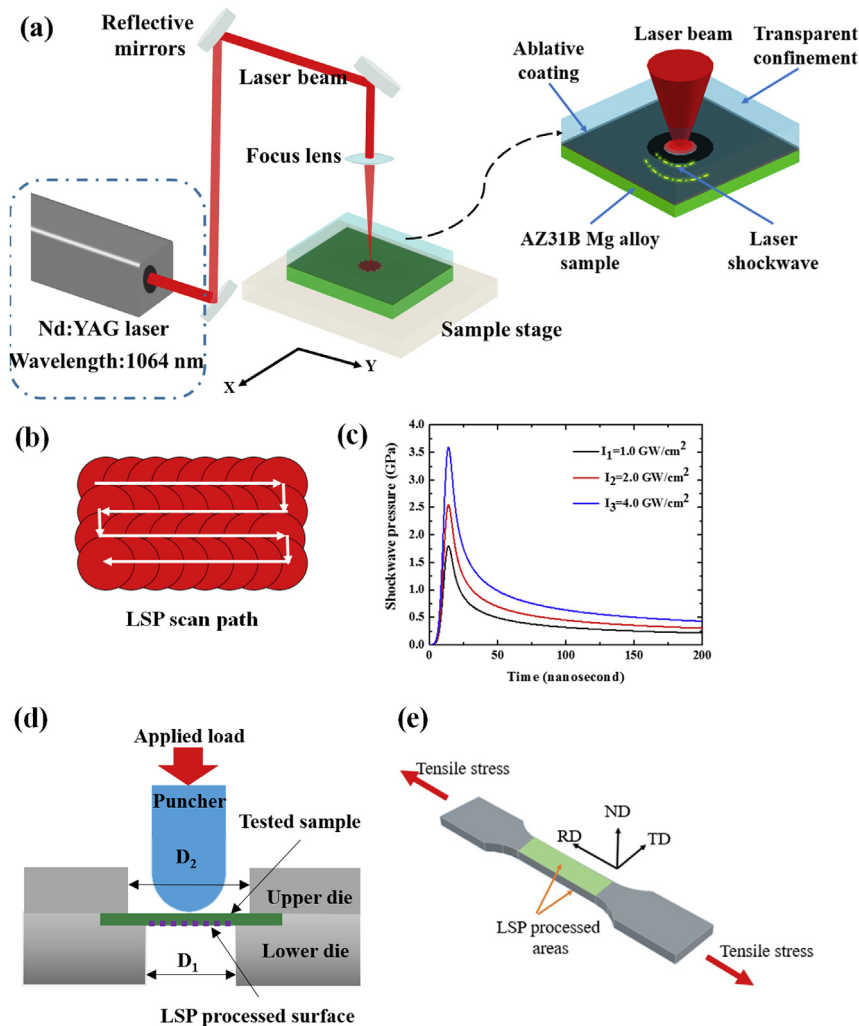

Fig. 1. (a) Schematic setup of the LSP process. (b) LSP scan path. (c) The temporal evolution of laser shockwave pressure as affected by the laser intensity in LSP experiments, estimated by Fabbro's model. Schematic configurations of the (d) Erichsen test and (e) tensile test.
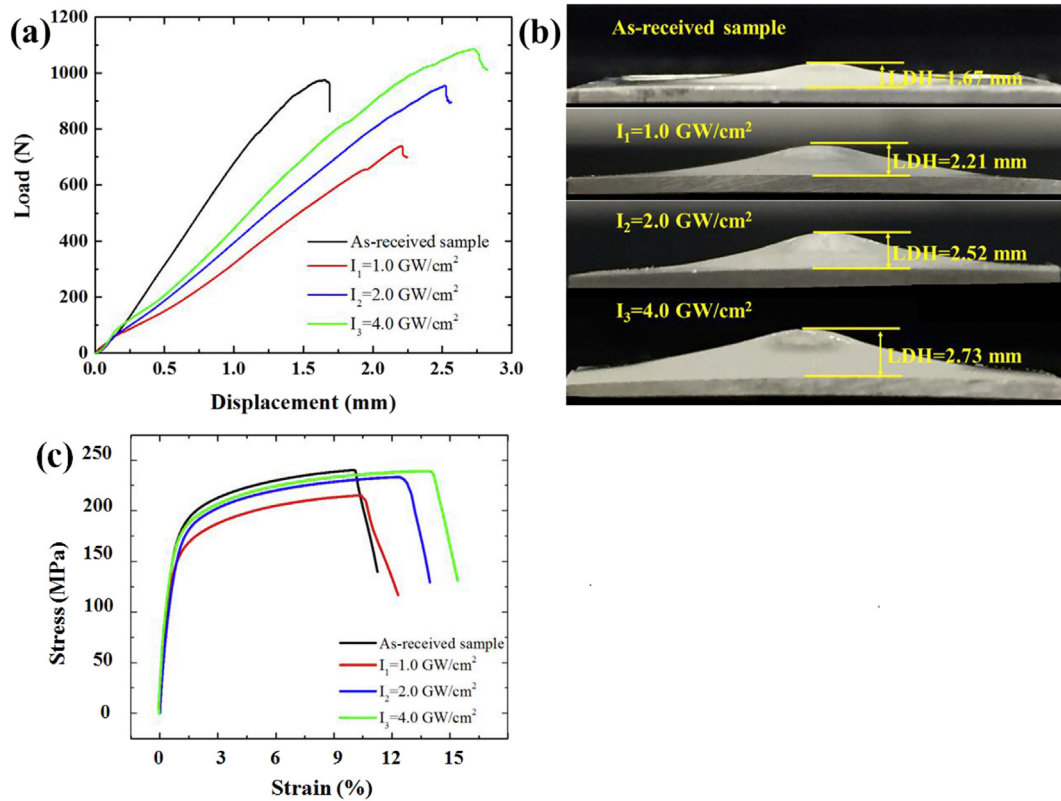
Fig. 2. (a) Load vs. displacement curves of unprocessed and LSP processed Mg alloy samples in the Erichsen tests. (b) Side view of the Mg alloy samples after Erichsen tests. (c) Tensile stress-strain curves of unprocessed and LSP processed Mg alloy samples.

3. Results and discussion

Results of the Erichsen tests are shown in Fig. 2. As observed in the load vs. displacement curves (Fig. 2a), LSP enhances stretch formability of Mg alloy sheet. As compared to the unprocessed sample, a lower load is needed for processed samples to reach the same displacement. For instance, to reach a deformation displacement of 1.0 mm, the load for sample processed by LSP with a laser intensity of 1.0 GW/cm^2 is 310 N, which is only 48% of the load used for unprocessed sample (650 N). In addition, the enhanced stretch formability is confirmed by the side view of the samples after Erichsen tests (Fig. 2b). It can be seen that the processed samples exhibit a higher value of LDH as compared to the unprocessed one. For instance, the unprocessed sample has a LDH value of 1.67 mm, whereas for the sample processed by LSP with a laser intensity of 4.0 GW/cm^2, the LDH value increases by 63% to 2.73 mm. Moreover, a higher laser intensity results in a higher LDH value. The value of LDH increases from 2.21 to 2.73 mm as the laser intensity increases from 1.0 to 4.0 GW/cm^2.

Tensile testing results are shown in Fig. 2c. It is observed that the yield strength and ultimate tensile strength (UTS) of LSP processed samples are lower than those of the unprocessed one, while the fracture elongation (FE) of LSP processed samples are greater than that of the unprocessed one. Moreover, both the UTS and FE increase with the increase of laser intensity. For instance, as the laser intensity increases from 1.0 to 4.0 GW/cm^2, the UTS increases from 212 to 241 MPa, and the FE increases from 10.5% to 13.8%.

To reveal the mechanism responsible for the enhanced formability of Mg alloys by LSP, EBSD analysis was performed. The inverse pole figure (IPF) maps, image quality maps, and pole figure maps of the surface of the unprocessed and processed samples are presented in Fig. 3a–d. It can be seen that the unprocessed sample exhibits a strong basal texture together with a twin-free equiaxial grain structure (Fig. 3a). After LSP, a high density of twin lamellas, mostly identified as

$\{10\bar{1}2\}10\bar{1}1$ extension twins (Fig. 3b–d), were generated. A higher laser intensity leads to a higher twin volume fraction (Fig. 3b–d). As an evidence of texture weakening effect, the pole figure maps show that the $\{0002\}$ poles spread along the RD after LSP and this trend becomes more apparent as the laser intensity increases due to the increase of twin volume fraction. Note that, the appearance of high density $\{10\bar{1}2\}$ twins in this study seems abnormal since its activation is most favorable when a tensile stress is applied along the c-axis or a compressive stress is applied perpendicular to the c-axis of Mg crystals [37]. In this study where a compressive stress is applied along c-axis, the activation of $\{10\bar{1}2\}$ twins should be suppressed (Fig. 3e). To address this paradox, single pulse LSP experiment with a laser intensity of 2.0 GW/cm^2 and a beam diameter of 2.0 mm was conducted on Mg alloy samples along ND. The microstructure of the processed surface was examined by OM (Fig. 3f–h). A donut-like distribution of twins can be identified in Fig. 3f, where the twinning zone is marked between the yellow and red dash lines. The twinned zone is located along the perimeter of laser processed area (Fig. 3h), while few twins can be found in the center area with a diameter equal to the diameter of laser beam (Fig. 3g). Similar findings have been reported in Refs. [38,39], in which the $\{10\bar{1}2\}$ twins tend to form on the perimetric area of an indentation where the stresses favor extension twinning. Therefore, in the continuous LSP experiment along ND where the sample surface is completely processed with a laser beam overlapping ratio of 75%, surface twinning with a high density can be achieved (as observed in Fig. 3d), leading to the texture weakening effect.

In addition, the cross-sectional microstructure (RD-ND plane) at a depth of 300 μm before and after LSP was characterized using EBSD (Fig. 4). The unprocessed sample (Fig. 4a) possesses a relatively homogenous distribution of equiaxed grains with a grain size of 20–40 μm, while the processed sample (Fig. 4b) exhibits a bimodal microstructure containing both coarse and fine grains. Grains with a size of a few microns can be found in Fig. 4b and c, indicating that the
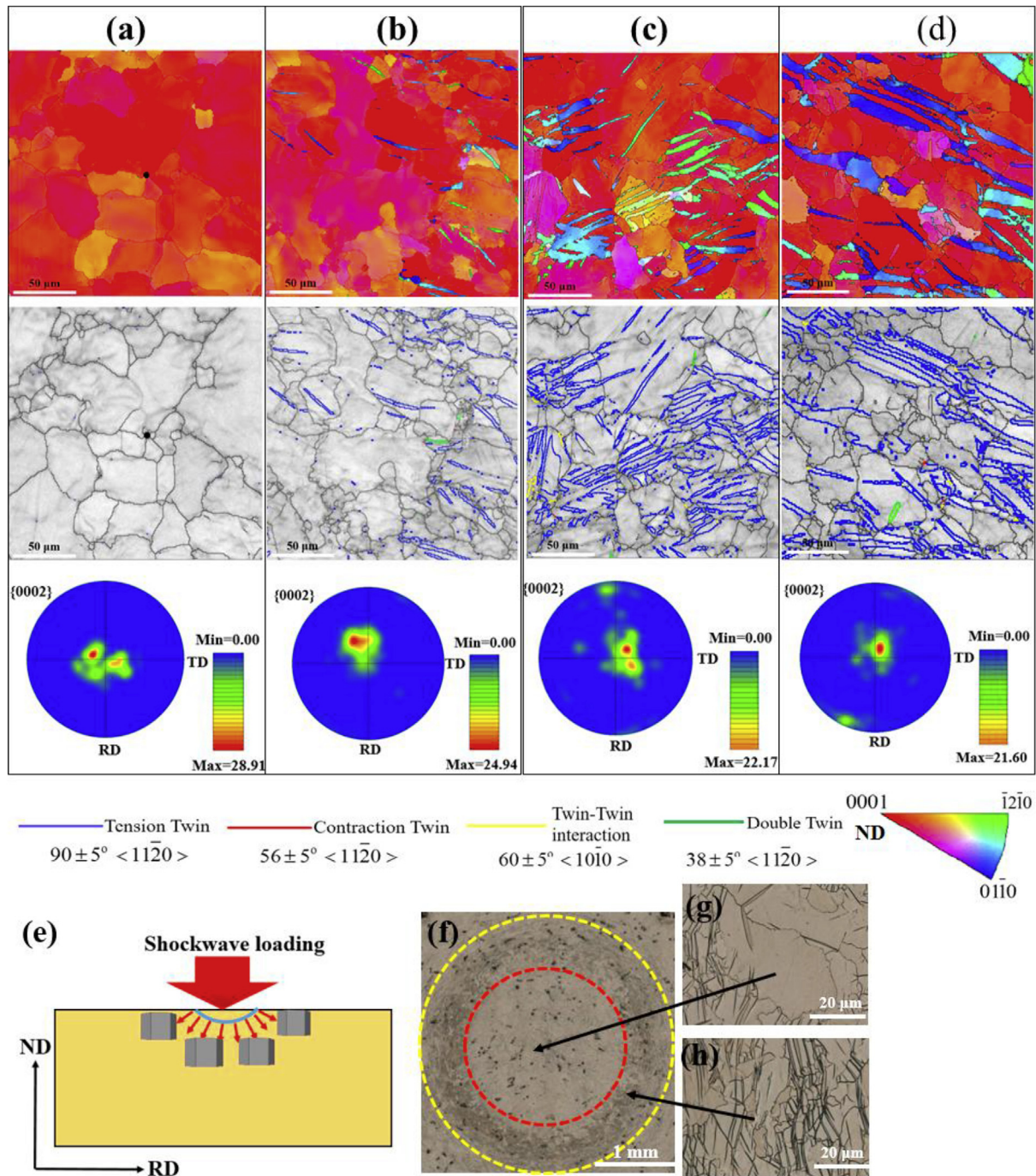
Fig. 3. EBSD analysis of the surface microstructure (perpendicular to ND) of the Mg alloy samples: (a) As-received sample, and samples processed by LSP with a laser intensity of (b) 1.0 GW/cm^2, (c) 2.0 GW/cm^2, and (d) 4.0 GW/cm^2. (e) Initial texture of the as-received sample and schematic of stress distribution during single pulse LSP. Optical microcopy images of the surface processed by single pulse LSP with a laser intensity of 2.0 GW/cm^2: (f) LSP created a donut-shaped zone. (g) Central area with few twins. (h) Perimetric area with a high density of twins.

grains were refined to a certain extent after LSP. IPF maps of some local areas with observable grain refinement are shown in Fig. 4d–h.

The grain refinement of metallic materials by LSP has been reported [23,32,33]. It is normally observed in the layer of severe plastic deformation right beneath the processed surface with a thickness of less than 100 μm. However, Fig. 4b–h demonstrate the grain refinement can occur at a depth around 400 μm in the LSP processed Mg alloys due to recrystallization. Twin lamellas can be identified in Fig. 4b and c. The image quality map (Fig. 4c) shows the dominant twin boundaries are $90 \pm 5°\langle11\bar{2}0\rangle$ (blue lines) representing $\{10\bar{1}2\}\langle10\bar{1}1\rangle$ extension twins and $38 \pm 5°\langle11\bar{2}0\rangle$ (green lines) representing $\{10\bar{1}1\} + \{10\bar{1}2\}$ double twins. It

is reported that $\{10\bar{1}2\}$ twins can serve as nucleation sites for dynamic recrystallization (DRX) during hot working [40]. Wang et al. [41] showed that deformation with a high strain rate promoted DRX of Mg alloys due to the elevated activities of deformation twinning. In LSP, the strain rate is as high as 10^6/s and the duration of laser shock loading is as short as 100 ns, the plastic work stored in a confined volume may trigger nucleation and growth of new grains. DRX can be proved by the misorientation angle distribution of the grain boundaries as shown in Fig. 4i. The peak intensity at a low misorientation angle of 5° is an indication of the extensive subgrain structures, whereas the misorientation peak at 30° is mainly attributed to the 30° $\langle0001\rangle$
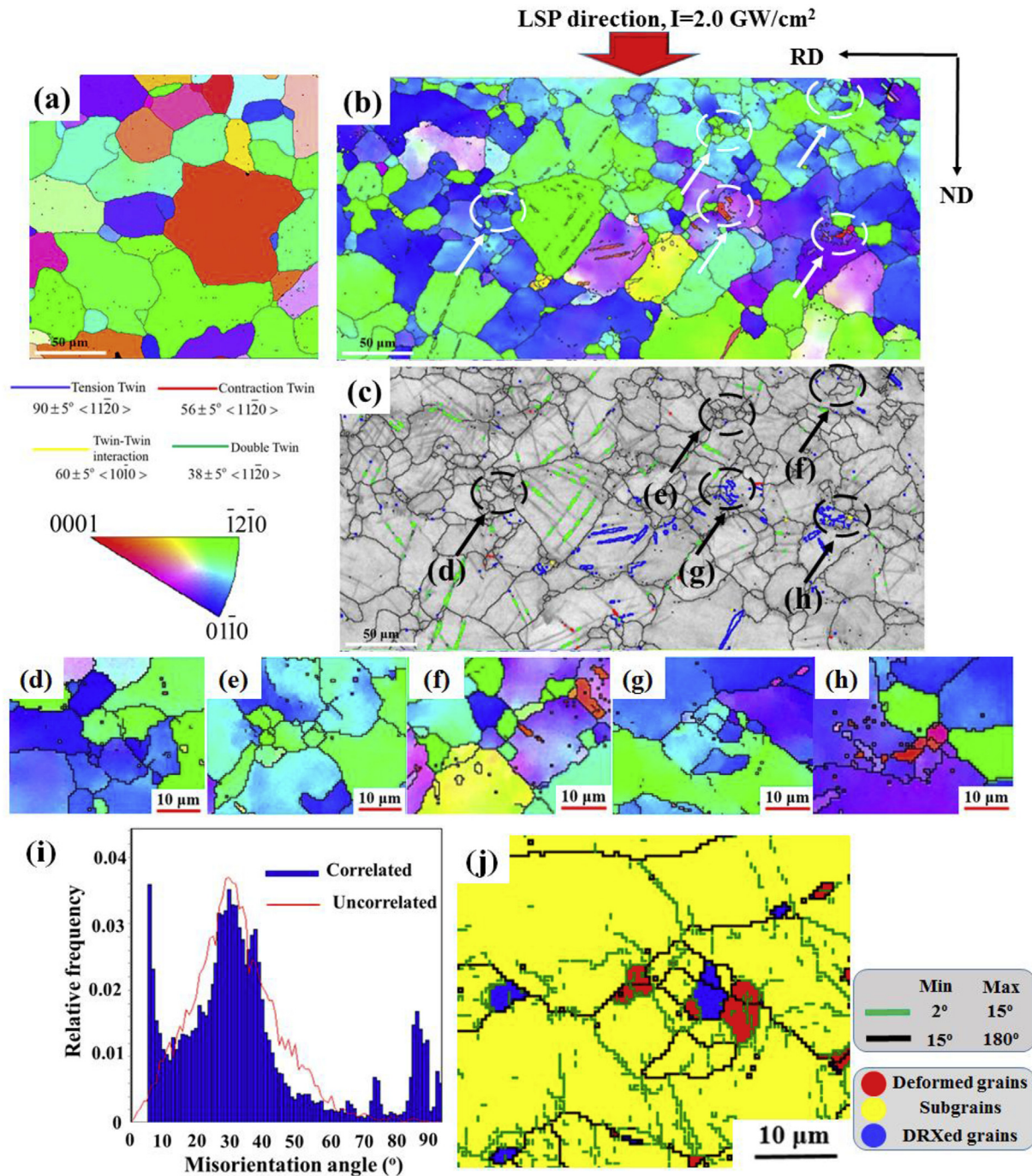
Fig. 4. EBSD analysis of the cross-sectional microstructure (ND-RD plane) of the Mg alloy samples: (a) IPF map of the as-received sample; (b) IPF map and (c) image quality map of the sample processed by continuous LSP with a laser intensity of 2.0 GW/cm^2; (d)–(h) IPF maps of some local areas showing significant grain refinement. (i) Corresponding misorientation angle distribution for (b). (j) EBSD maps distinguishing the DRXed grains (blue area), subgrains (yellow area), and deformed grains (red area) for (g). (For interpretation of the references to colour in this figure legend, the reader is referred to the Web version of this article.)

misorientation relationship during the growth of DRXed grains [42,43]. In Fig. 4j, EBSD analysis was used to distinguish the deformed grains, sub-grains, and recrystallized grains, following the method used in Refs. [44–46]. Large amounts of subgrains with extensive low angle grain boundaries and several DRXed grains with an average grain size around 3 μm can be identified.

Based on the microstructural analysis, the mechanism responsible for the improved formability of Mg alloys by LSP can be proposed. During the Erichsen test, biaxial tensile stress field is applied on sample sheet [47,48]. The microstructure of the LSP processed samples is composed of a mixture of parent grains, twinned grains and refined grains. For the parent grains, the compressive strain along the thickness direction activates pyramidal $c + a$ slip or contraction twinning, whose critical resolve shear stresses are higher than those of a slip (basal and prismatic) or extension twinning. Therefore, deformation of rolled Mg alloys with a strong basal texture along the thickness direction is difficult, leading to a poor stretch formability. In contrast, for the twinned grains with crystallographic orientation rotated by ~90°, "re-twinning" [31], or "de-twinning" [49] can be activated to accommodate the plastic strain, enabling an easier and more homogenous plastic deformation. For polycrystalline materials, individual crystals deform only along specific crystallographic orientations, thus deformation

compatibility among grains is often required to accommodate the macroscopic shape changes [50,51]. In this regard, the weakened basal texture induced by pre-twinning contributes to the deformation compatibility and improves the stretch formability. Moreover, the refined grains induced by LSP could provide additional plastic deformation modes, i. e., grain boundary sliding (GBS), leading to the improved stretch formability [52]. GBS has been perceived as important approach to realize the superplasticity of metals. Despite that GBS often occurs at elevated temperatures, recent studies [53–55] indicate that it can be activated in Mg alloys at room temperature once the grain size is reduced to one micron or sub-micron, leading to significantly improved formability. In our study, plastic stain can be accommodated through the above discussed mechanisms. As the laser intensity increases, more refined grains are generated, leading to the decrease of average grain size. As a result, according to the Hall-Petch relationship [56,57], the grain boundary hardening effect leads to the increase of the stress required for plastic deformation. Therefore, both the loading forces in load-displacement curves (Fig. 2a) and strength levels in stress-strain curves (Fig. 2c) increase with the increase of laser intensity.

4. Conclusion

In summary, enhanced room-temperature stretch formability of Mg alloy sheet by LSP is investigated. The results show the formability of Mg alloys can be increased by 63%. Based on the microstructural analysis, a combination of texture weakening by extension twinning and grain refinement induced by LSP may account for the improved stretch formability of the Mg alloy.

Acknowledgements

References

[1] T.M. Pollock, Weight loss with magnesium alloys, Science 328 (2010) 986–987.

[2] G.S. Frankel, Magnesium alloys: ready for the road, Nat. Mater. 14 (2015) 1189.

[3] Z. Wu, R. Ahmad, B. Yin, S. Sandlöbes, W. Curtin, Mechanistic origin and prediction of enhanced ductility in magnesium alloys, Science 359 (2018) 447–452.

[4] Z. Wu, W. Curtin, The origins of high hardening and low ductility in magnesium, Nature 526 (2015) 62.

[5] N. Stanford, K. Sotoudeh, P. Bate, Deformation mechanisms and plastic anisotropy in magnesium alloy AZ31, Acta Mater. 59 (2011) 4866–4874.

[6] Y. Chino, M. Kado, M. Mabuchi, Enhancement of tensile ductility and stretch formability of magnesium by addition of 0.2 wt%(0.035 at%) Ce, Mater. Sci. Eng., A 494 (2008) 343–349.

[7] D. Wu, R. Chen, E. Han, Excellent room-temperature ductility and formability of rolled Mg–Gd–Zn alloy sheets, J. Alloy. Comp. 509 (2011) 2856–2863.

[8] Y. Chino, K. Sassa, M. Mabuchi, Texture and stretch formability of a rolled Mg–Zn alloy containing dilute content of Y, Mater. Sci. Eng., A 513 (2009) 394–400.

[9] S. Masoudpanah, R. Mahmudi, Effects of rare-earth elements and Ca additions on the microstructure and mechanical properties of AZ31 magnesium alloy processed by ECAP, Mater. Sci. Eng., A 526 (2009) 22–30.

[10] N. Stanford, D. Atwell, A. Beer, C. Davies, M. Barnett, Effect of microalloying with rare-earth elements on the texture of extruded magnesium-based alloys, Scripta Mater. 59 (2008) 772–775.

[11] K. Hantzsche, J. Bohlen, J. Wendt, K. Kainer, S. Yi, D. Letzig, Effect of rare earth additions on microstructure and texture development of magnesium alloy sheets, Scripta Mater. 63 (2010) 725–730.

[12] S. Sandlöbes, M. Friák, S. Korte-Kerzel, Z. Pei, J. Neugebauer, D. Raabe, A rare-earth free magnesium alloy with improved intrinsic ductility, Sci. Rep. 7 (2017) 10458.

[13] B. Song, R. Xin, A. Liao, W. Yu, Q. Liu, Enhancing stretch formability of rolled Mg sheets by pre-inducing contraction twins and recrystallization annealing, Mater. Sci. Eng., A 627 (2015) 369–373.

[14] X. Huang, K. Suzuki, Y. Chino, M. Mabuchi, Improvement of stretch formability of Mg–3Al–1Zn alloy sheet by high temperature rolling at finishing pass, J. Alloy. Comp. 509 (2011) 7579–7584.

[15] X. Huang, K. Suzuki, A. Watazu, I. Shigematsu, N. Saito, Improvement of formability of Mg–Al–Zn alloy sheet at low temperatures using differential speed rolling, J. Alloy. Comp. 470 (2009) 263–268.

[16] X. Li, F. Wang, X. Li, G. Tang, J. Zhu, Improvement of formability of Mg–3Al–1Zn

[17] Q. Huo, X. Yang, H. Sun, B. Li, J. Qin, J. Wang, et al., Enhancement of tensile ductility and stretch formability of AZ31 magnesium alloy sheet processed by cross-wavy bending, J. Alloy. Comp. 581 (2013) 230–235.

[18] J. Suh, J. Victoria-Hernández, D. Letzig, R. Golle, W. Volk, Enhanced mechanical behavior and reduced mechanical anisotropy of AZ31 Mg alloy sheet processed by ECAP, Mater. Sci. Eng., A 650 (2016) 523–529.

[19] V.M. Miller, T.D. Berman, I.J. Beyerlein, J.W. Jones, T.M. Pollock, Prediction of the plastic anisotropy of magnesium alloys with synthetic textures and implications for the effect of texture on formability, Mater. Sci. Eng., A 675 (2016) 345–360.

[20] Z. Zeng, J.-F. Nie, S.-W. Xu, H.J. Davies C, N. Birbilis, Super-formable pure magnesium at room temperature, Nat. Commun. 8 (2017) 972.

[21] B. Mao, Y. Liao, B. Li, Gradient twinning microstructure generated by laser shock peening in an AZ31B magnesium alloy, Appl. Surf. Sci. 457 (2018) 342–351.

[22] R. Zhang, X. Zhou, H. Gao, S. Mankoci, Y. Liu, X. Sang, et al., The effects of laser shock peening on the mechanical properties and biomedical behavior of AZ31B magnesium alloy, Surf. Coating. Technol. 339 (2018) 48–56.

[23] M.-Z. Ge, J.-Y. Xiang, Effect of laser shock peening on microstructure and fatigue crack growth rate of AZ31B magnesium alloy, J. Alloy. Comp. 680 (2016) 544–552.

[24] B. Mao, A. Siddaiah, X. Zhang, B. Li, P.L. Menezes, Y. Liao, The influence of surface pre-twinning on the friction and wear performance of an AZ31B Mg alloy, Appl. Surf. Sci. 480 (2019) 998–1007.

[25] X. Li, Y. Zhang, J. Chen, Y. Lu, Effect of laser shock processing on stress corrosion cracking behaviour of AZ31 magnesium alloy at slow strain rate, Mater. Sci. Technol. 29 (2013) 626–630.

[26] P. Peyre, R. Fabbro, Laser shock processing: a review of the physics and applications, Opt. Quant. Electron. 27 (1995) 1213–1229.

[27] C.S. Montross, T. Wei, L. Ye, G. Clark, Y.-W. Mai, Laser shock processing and its effects on microstructure and properties of metal alloys: a review, Int. J. Fatigue 24 (2002) 1021–1036.

[28] M. Barnett, Twinning and the ductility of magnesium alloys: Part I: "Tension" twins, Mater. Sci. Eng., A 464 (2007) 1–7.

[29] B. Mao, Y. Liao, B. Li, Abnormal twin-twin interaction in an Mg-3Al-1Zn magnesium alloy processed by laser shock peening, Scripta Mater. 165 (2019) 89–93.

[30] B. Song, N. Guo, T. Liu, Q. Yang, Improvement of formability and mechanical properties of magnesium alloys via pre-twinning: a review, Mater. Des. 62 (2014) 352–360 1980-2015.

[31] W. He, Q. Zeng, H. Yu, Y. Xin, B. Luan, Q. Liu, Improving the room temperature stretch formability of a Mg alloy thin sheet by pre-twinning, Mater. Sci. Eng., A 655 (2016) 1–8.

[32] X. Ren, J. Huang, W. Zhou, S. Xu, F. Liu, Surface nano-crystallization of AZ91D magnesium alloy induced by laser shock processing, Mater. Des. 86 (2015) 421–426.

[33] X. Ren, X. Yang, W. Zhou, J. Huang, Y. Ren, C. Wang, et al., Thermal Stability of Surface Nano-Crystallization Layer in AZ91D Magnesium Alloy Induced by Laser Shock Peening, Surface and Coatings Technology, 2017.

[34] B. Mao, A. Siddaiah, P.L. Menezes, Y. Liao, Surface texturing by indirect laser shock surface patterning for manipulated friction coefficient, J. Mater. Process. Technol. 257 (2018) 227–233.

[35] A. Siddaiah, B. Mao, Y. Liao, P.L. Menezes, Surface characterization and tribological performance of laser shock peened steel surfaces, Surf. Coating. Technol. 351 (2018) 188–197.

[36] R. Fabbro, P. Peyre, L. Berthe, X. Scherpereel, Physics and applications of laser-shock processing, J. Laser Appl. 10 (1998) 265–279.

[37] J.W. Christian, S. Mahajan, Deformation twinning, Prog. Mater. Sci. 39 (1995) 1-157.

[38] B. Selvarajou, J.-H. Shin, T.K. Ha, I-s Choi, S.P. Joshi, H.N. Han, Orientation-dependent indentation response of magnesium single crystals: modeling and experiments, Acta Mater. 81 (2014) 358–376.

[39] J.-H. Shin, S.-H. Kim, T. Ha, K. Oh, I.-S. Choi, H. Han, Nanoindentation study for deformation twinning of magnesium single crystal, Scripta Mater. 68 (2013) 483–486.

[40] Q. Ma, B. Li, E. Marin, S. Horstemeyer, Twinning-induced dynamic recrystallization in a magnesium alloy extruded at 450 C, Scripta Mater. 65 (2011) 823–826.

[41] T. Wang, J.J. Jonas, S. Yue, Dynamic recrystallization behavior of a coarse-grained Mg-2Zn-2Nd magnesium alloy, Metall. Mater. Trans. 48 (2017) 594–600.

[42] R.K. Nadella, I. Samajdar, G. Gottstein, Static recrystallisation and textural changes in warm rolled pure magnesium, Magnesium: Proceedings of the 6th International Conference Magnesium Alloys and Their Applications, Wiley Online Library, 2003, pp. 1052–1057.

[43] T. Al-Samman, K.D. Molodov, D.A. Molodov, G. Gottstein, S. Suwas, Softening and dynamic recrystallization in magnesium single crystals during c-axis compression, Acta Mater. 60 (2012) 537–545.

[44] M. Jiang, C. Xu, H. Yan, S. Lu, T. Nakata, C. Lao, et al., Correlation between dynamic recrystallization and formation of rare earth texture in a Mg-Zn-Gd magnesium alloy during extrusion, Sci. Rep. 8 (2018) 16800.

[45] Q. Liu, J. Song, F. Pan, J. She, S. Zhang, P. Peng, The edge crack, texture evolution, and mechanical properties of Mg-1Al-1Sn-Mn alloy sheets prepared using on-line heating rolling, Metals 8 (2018) 860.

[46] F. Pan, B. Zeng, B. Jiang, M. Zhang, H. Dong, Enhanced mechanical properties of AZ31B magnesium alloy thin sheets processed by on-line heating rolling, J. Alloy. Comp. 693 (2017) 414–420.

[47] C. Hyun, M. Kim, S.-H. Choi, K. Shin, Crystal plasticity FEM study of twinning and slip in a Mg single crystal by Erichsen test, Acta Mater. 156 (2018) 342–355.

[48] B. Mao, Y. Liao, Modeling of lüders elongation and work hardening behaviors of

ferrite-pearlite dual phase steels under tension, Mech. Mater. 129 (2019) 222–229.

[49] S.H. Park, S.-G. Hong, C.S. Lee, Enhanced stretch formability of rolled Mg–3Al–1Zn alloy at room temperature by initial {10–12} twins, Mater. Sci. Eng., A 578 (2013) 271–276.

[50] J. Koike, R. Ohyama, T. Kobayashi, M. Suzuki, K. Maruyama, Grain-boundary sliding in AZ31 magnesium alloys at room temperature to 523 K, Mater. Trans. 44 (2003) 445–451.

[51] A. Orozco-Caballero, D. Lunt, J.D. Robson, J.Q. da Fonseca, How magnesium accommodates local deformation incompatibility: a high-resolution digital image correlation study, Acta Mater. 133 (2017) 367–379.

[52] W.-J. Kim, S. Chung, C. Chung, D. Kum, Superplasticity in thin magnesium alloy sheets and deformation mechanism maps for magnesium alloys at elevated temperatures, Acta Mater. 49 (2001) 3337–3345.

[53] H. Somekawa, A. Singh, Superior room temperature ductility of magnesium dilute binary alloy via grain boundary sliding, Scripta Mater. 150 (2018) 26–30.

[54] H. Somekawa, D.A. Basha, A. Singh, Room temperature grain boundary sliding behavior of fine-grained Mg-Mn alloys, Mater. Sci. Eng., A 730 (2018) 355–362.

[55] H. Somekawa, A. Kinoshita, K. Washio, A. Kato, Enhancement of room temperature stretch formability via grain boundary sliding in magnesium alloy, Mater. Sci. Eng., A 676 (2016) 427–433.

[56] W. Yuan, S. Panigrahi, J.-Q. Su, R. Mishra, Influence of grain size and texture on Hall–Petch relationship for a magnesium alloy, Scripta Mater. 65 (2011) 994–997.

[57] J. Del Valle, F. Carreño, O.A. Ruano, Influence of texture and grain size on work hardening and ductility in magnesium-based alloys processed by ECAP and rolling, Acta Mater. 54 (2006) 4247–4259.